Journal of *Marine Science and Engineering*

MDPI

Article

Factors Influencing the Spatio-Temporal Distribution of Chlorophyll-a in Jinmeng Bay, China

Dan Wang [1], Cuiping Kuang [1,*], Gang Wang [2,*], Jiantao Liu [2], Wei Song [3,4], Rongrong Xing [2] and Qingping Zou [5,*]

[1] College of Civil Engineering, Tongji University, Shanghai 200092, China; 1910282@tongji.edu.cn
[2] The Eighth Geological Brigade, Hebei Geological and Mineral Exploration Development Bureau, Qinhuangdao 066001, China; tao6031@126.com (J.L.); rrxing01@163.com (R.X.)
[3] Key Laboratory of Science and Engineering for Marine Ecology and Environment, The First Institute of Oceanography, Ministry of Natural Resources of People's Republic of China, Qingdao 266061, China; songw@fio.org.cn
[4] Laboratory of Marine Ecology and Environmental Science, Qingdao National Laboratory for Marine Science and Technology, Qingdao 266237, China
[5] The Lyell Centre for Earth and Marine Science and Technology, Institute for Infrastructure and Environment, Heriot-Watt University, Edinburgh EH14 4AS, UK
* Correspondence: cpkuang@tongji.edu.cn (C.K.); wanggang8080@163.com (G.W.); q.zou@hw.ac.uk (Q.Z.)

Abstract: Field observations were combined with a coupled hydrodynamic and water quality model to investigate the spatial and temporal variation in Chlorophyll-a (Chl-a) in Jinmeng Bay, China. The relatively high Chl-a values were distributed in the inshore waters, mainly due to the abundant nutrient inflow from the Tanghe River. The model's results indicate that the Chl-a concentration was much higher in seaweed beds surrounded by artificial islands and reefs under the southeasterly wind, largely due to the fact that pollutants are prone to accumulate in coastal areas where flow is attenuated by the presence of natural and artificial marine structures. It was also found that the southwesterly winds suppress the inflow of nutrients from the Tanghe River to the coastal areas, and, therefore, lower the Chl-a levels. River input and wind forcing are the major factors that influence Chl-a concentrations in the anthropogenically influenced bay. This finding provides useful guidance for the prediction and mitigation of green tides in Jinmeng Bay in the future.

Keywords: Chlorophyll-a concentration; numerical modeling; nutrients; residual current; wind

check for updates

Citation: Wang, D.; Kuang, C.; Wang, G.; Liu, J.; Song, W.; Xing, R.; Zou, Q. Factors Influencing the Spatio-Temporal Distribution of Chlorophyll-a in Jinmeng Bay, China. *J. Mar. Sci. Eng.* **2024**, *12*, 384. https://doi.org/10.3390/jmse12030384

Academic Editor: Terry E. Whitledge

Received: 5 January 2024
Revised: 27 January 2024
Accepted: 21 February 2024
Published: 23 February 2024

Copyright: © 2024 by the authors. Licensee MDPI, Basel, Switzerland. This article is an open access article distributed under the terms and conditions of the Creative Commons Attribution (CC BY) license (https://creativecommons.org/licenses/by/4.0/).

1. Introduction

Green tides have recurred annually since 2015 along the famous tourist beaches of Jinmeng Bay, Bohai Sea. Massive algae, including *Ulva pertusa*, *Bryopsis plumosa* and *Ulva prolifera*, accumulated on the shore resulting in environmental degradation and economic losses [1–4]. Every year, from 2015 to 2019, the annual green tide bloom in Jinmeng Bay started in late April from seaweed beds, reached a peak in July and August, and eventually disappeared from the sea surface at the end of September [4,5]. However, during July 2020, the green tide magnitude decreased by a biomass of 151 g/m^3, or one-thirtieth, compared to previous years due to multiple factors (e.g., micro-propagules and nutrients) [5]. Chlorophyll-a (Chl-a) has been used as an index to quantify the proliferation of algal blooms and marine water quality [6–9].

Previous studies have suggested several driving factors for the Chl-a distribution [10–15]. For instance, the long-term Chl-a change in the Bohai and Yellow Seas was closely related to the eutrophication of seawater [16]. Chl-a concentrations displayed significant correlations with wind speed in areas of shallow mixed layers, because high winds deepen mixed layers and drive more nutrients into the upper ocean [17]. Nababan et al. [18] attributed the high Chl-a concentrations in the northeastern Gulf of Mexico to river discharges and wind

induced upwelling. Horizontal advection contributes to the high Chl-a concentrations along the east coast of Vietnam [19].

The numerical model is approved as an efficient method to study the aquatic ecosystem, including the transport and cycling of nutrients, and major chemical and biological processes in waters [20–25]. By establishing a 3D hydro-ecological model, Gao et al. [26] studied the principal reason for frequent phytoplankton blooms in Xiangxi Bay, and found that the Chl-a concentration can be estimated using water age and water temperature. Cruz-Rico and Rivas [27] suggested that the changes in Chl-a in the Todos Santos Bay were associated with the Pacific Decadal Oscillation using the numerical model. Yu et al. [28] applied a three-dimensional ecosystem model to examine the spatial distribution of nutrients and Chl-a biomass in Laizhou Bay. Feng et al. [29] found that relatively low wind velocities determined the high accumulation of Bacillariophyta in the Douhe Reservoir based on a mathematical model. Lopes et al. [30] investigated the seasonal variation of nutrients in the Ria de Aveiro Lagoon by coupling hydrodynamics and the water quality module.

Green tides can cause serious impacts to ecosystems in an important resort area such as Jinmeng Bay. Previous studies mainly focused on the roles of micro-propagules during green tide development and the molecular identification of the dominant species [4,5]. There is a lack of water quality studies in the green tide areas in Jinmeng Bay, especially the spatiotemporal variation of Chl-a near the bay. Field surveys and a coupled hydrodynamic-water quality model were carried out to investigate the mechanisms for controlling the spatio-temporal distributions of Chl-a in Jinmeng Bay in this study. The objectives were (1) to assess the characteristics of the spatial and temporal distributions of Chl-a; (2) to evaluate the variation trends of nutrients in the Tanghe River; and (3) to identify the key factors influencing Chl-a dynamics.

2. Materials and Methods

2.1. Study Area

Jinmeng Bay, surrounded by multiple artificial structures, is an anthropogenically influenced bay in the Bohai Sea, China (Figure 1). Lotus Island, submerged breakwaters, and Conch Island have been successively built since 2011. The currents in the nearshore waters were obviously weakened by the artificial structures (~0.3 m/s), with an average water exchange period of 22 days. Jinmeng Bay is mainly dominated by a regular diurnal tide while the tidal currents are regular semi-diurnal type. The bay is relatively shallow (water depth < 13 m) and the turbidity in the southeast of Lotus Island is about 13.5 NTU. The sea surface temperature remained suitable (12–26 °C) from April to September for the green tides, which is a principal factor influencing species succession in Jinmeng Bay. The dominant species are *Ulva pertusa*, *Bryopsis plumosa*, and *Ulva prolifera*, in turn, during the process of blooms. Enormous macroalgae accumulated in the nearshore waters of Jinmeng Bay, and some macroalgae migrated southwestward along the coastline and affected other bathing beaches, including Jinwu, Qianshuiwan, and Geziwo.

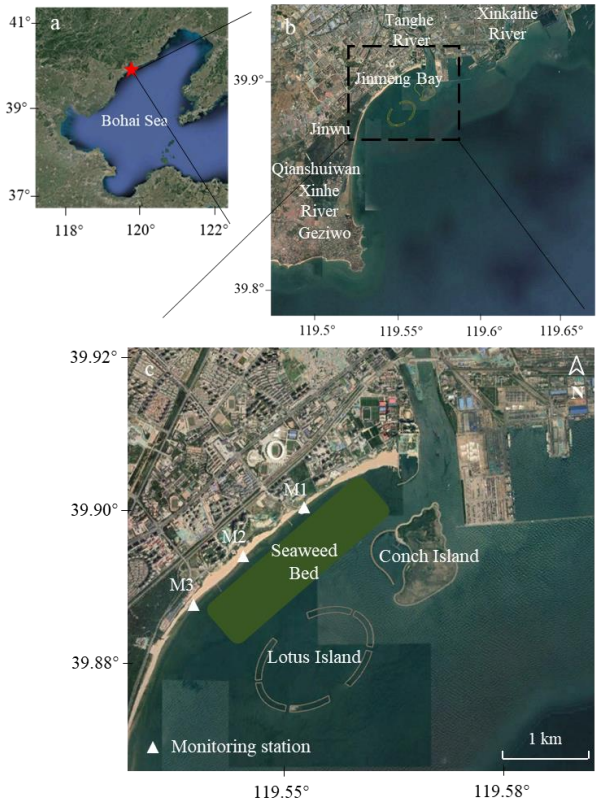

Figure 1. (**a**) Location of the study region, (**b**) the areas affected by the green tides including 4 bathing beaches (Jinmeng Bay, Jinwu, Qianshuiwan, and Geziwo), (**c**) zoomed in view of the locations of the seaweed beds and field observations indicated by the black rectangular box in (**b**). The triangles indicate sampling stations in the bay for floating macroalgae analyses. Green shadow areas indicate the seaweed beds.

2.2. Model Description

Mike 21 Flow Model FM was applied to study the hydrodynamics of Jinmeng Bay [31]. MIKE 21 Flow Model FM has been used for applications in various aspects of physical and biological oceanography [32–36]. The model, based on incompressible Reynolds averaged Navier–Stokes equations, Boussinesq assumption and hydrostatic pressure, consists of continuity and momentum equations.

$$\frac{\partial h}{\partial t} + \frac{\partial hu}{\partial x} + \frac{\partial hv}{\partial y} = hS \tag{1}$$

$$\frac{\partial hu}{\partial t} + \frac{\partial hu^2}{\partial x} + \frac{\partial hvu}{\partial y} = fvh - gh\frac{\partial \eta}{\partial x} - \frac{h}{\rho_0}\frac{\partial P_a}{\partial x} - \frac{gh^2}{2\rho_0}\frac{\partial \rho}{\partial x} + \frac{\tau_{sx}}{\rho_0} - \frac{\tau_{bx}}{\rho_0} + F_u + hu_S S \tag{2}$$

$$\frac{\partial hv}{\partial t} + \frac{\partial huv}{\partial x} + \frac{\partial hv^2}{\partial y} = -fuh - gh\frac{\partial \eta}{\partial y} - \frac{h}{\rho_0}\frac{\partial P_a}{\partial y} - \frac{gh^2}{2\rho_0}\frac{\partial \rho}{\partial y} + \frac{\tau_{sy}}{\rho_0} - \frac{\tau_{by}}{\rho_0} + F_v + hv_S S \tag{3}$$

where t is the time; x, y are the Cartesian co-ordinates; $h = d + \eta$ is the total water depth; u, v are the velocity components in the x and y direction; S is the magnitude of the source and (u_S, v_S) is the velocity components of the source; f is the Coriolis parameter; g is the gravitational acceleration; P_a is the atmospheric pressure; ρ and ρ_0 are the density and reference density of water; $(\tau_{sx}, \tau_{\mathrm{sy}})$ and (τ_{bx}, τ_{by}) are the x and y components of the surface wind and bottom stresses; F_u and F_v are horizontal stress terms dominated by sub-grid scale Samagorinsky horizontal eddy viscosity.

Wind stress is an important driver force for the circulation in Jinmeng Bay [37], given by:

$$\tau_S = \rho_a c_f |u_w| u_w \tag{4}$$

$$c_f = \begin{cases} c_a & u_w < w_a \\ c_a + \frac{c_b - c_a}{w_b - w_a}(u_w - w_a) & w_a \le u_w < w_b \\ c_b & u_w \ge w_b \end{cases} \tag{5}$$

where ρ_a is the density of air; u_w is the wind speed 10 m above the surface; c_f is the drag coefficient depending on the wind speed; and c_a, c_b, w_a and w_b are empirical factors with default values of 0.001255, 0.002425, 7 m/s and 25 m/s, respectively.

The water quality was simulated utilizing the output (e.g., water level and currents) from the hydrodynamics model to calculate the concentrations of nutrients and Chl-a [38–40]. In this study, dissolved oxygen (DO), biological oxygen demand (BOD_5), nitrate (NO_3-N), nitrite (NO_2-N), ammonium (NH_4-N), phosphate (PO_4-P), and Chl-a were calculated. A total of 19 processes and 36 constants are considered to describe photosynthesis, respiration, nitrification, denitrification, etc. The mass balance for Chl-a can be described by:

$$\frac{\mathrm{dCHL}}{\mathrm{dt}} = (\mathrm{P_{max}} \cdot \cos 2\pi(\tau/\alpha) \cdot {\theta_1}^{\mathrm{T}-20} - R_1 \cdot {\theta_2}^{\mathrm{T}-20}) \cdot \mathrm{K_1} \cdot \mathrm{K_2} \cdot \mathrm{F(N,P)} - \mathrm{K_3} \cdot \mathrm{CHL} - \mathrm{K_4/h} \cdot \mathrm{CHL} \tag{6}$$

where CHL is the concentration of Chl-a (mg/L); P_{max} is the rate of oxygen production by photosynthesis (g/m^2/d); θ_1 is the Arrhenius temperature coefficient for oxygen demand; τ is the actual time of the day; α is the relative daylength; R_1 is the respiration rate of plants (d^{-1}); θ_2 is the temperature coefficient for oxygen respiration; K_1 and K_2 are the carbon to oxygen ratio at primary production and Chl-a to carbon ratio, respectively; K_3 is the death rate of Chl-a (d^{-1}); K_4 is the settling rate of Chl-a (m/d); T is the water temperature (°C); and F(N,P) is the nutrient limitation function given by:

$$\mathrm{F(N,P)} = \frac{2 \cdot \left(\frac{\mathrm{IN}}{\mathrm{IN} + \mathrm{KSN}} \cdot \frac{\mathrm{PO_4}}{\mathrm{PO_4} + \mathrm{KSP}}\right)}{\left(\frac{\mathrm{IN}}{\mathrm{IN} + \mathrm{KSN}} + \frac{\mathrm{PO_4}}{\mathrm{PO_4} + \mathrm{KSP}}\right)} \tag{7}$$

where IN represents the dissolved inorganic nitrogen, and it is the sum concentrations of NO_3-N, NO_2-N and NH_4-N; PO_4 is the concentration of PO_4-P (mg/L); KSN is the half-saturation concentration for nitrogen; and KSP is the half-saturation concentration for phosphorus.

2.3. Model Configuration

To resolve the artificial islands in the study area, an unstructured mesh (triangular grid) was used to represent the complex geometry of Jinmeng Bay (Figure 2). A total of 5969 nodes and 10,986 elements were applied in the region, and the mesh size decreased from 4 km in the open sea to 8 m nearshore. Considering the effectiveness and accuracy during the calculation, a hydrodynamic model was established on the triple-nested grids as described in our previous study [37].

For the hydrodynamic model, wet-dry dynamic boundary processing technology was adopted, and the critical water depths of dry and wet points were 0.005 m and 0.05 m, respectively. Wind forcing for 2020 was taken from the hourly data of the European Centre for Medium-Range Weather Forecast. The bed resistance was determined by using the Manning number, with a mean value of 74 m$^{1/3}$/s.

The water quality model consists of the advection-diffusion equations for the transport of DO, BOD_5, NO_3-N, NO_2-N, NH_4-N, PO_4-P and Chl-a. In this study, the scaled eddy viscosity formulation dependent on the Prandtl number was selected to define the horizontal dispersion, which is set to 1 by calibration. Some key parameters were adjusted, including ratio of NH_4-N released by BOD decay, PO_4-P content in BOD, and the degrada-

tion constant for organic matter (0.25, 0.0055 and 0.05/d, respectively). The river boundary was defined by the measurement data of NO_3-N, NH_4-N, and PO_4-P, etc.

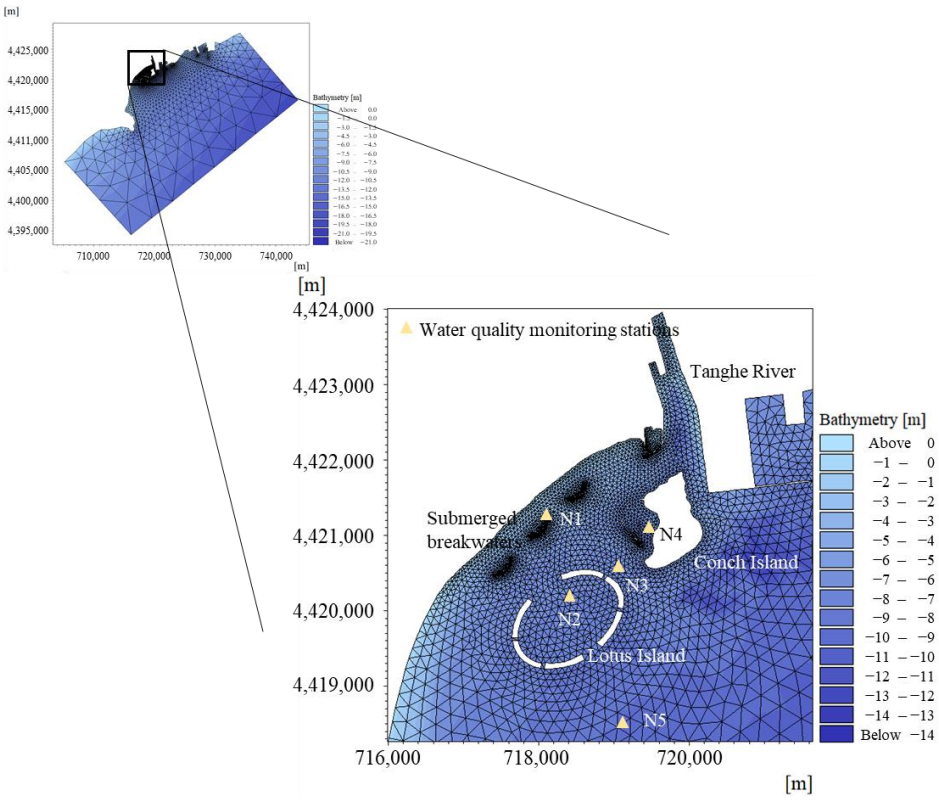

Figure 2. Bathymetry and mesh of Jinmeng Bay. Yellow triangles denote water quality observation stations (labeled with a station number).

2.4. Model Validation

The hydrodynamic model is considered to be relatively accurate and reliable in predicting the flow field in Jinmeng Bay. Our previous work provides a more detailed description and validation of the hydrodynamic model [37]. Bathymetric information of the study area was measured by Hebei Geological and Mineral Exploration Development Bureau. Environmental factors were obtained from field surveys by the Key Laboratory of Science and Engineering for Marine Ecology and Environment, The First Institute of Oceanography, China. Measurements of nutrients (e.g., NO_3-N, NH_4-N and PO_4-P) were collected in polypropylene bottles and analyzed by an AutoAnalyzer (AA3, Bran and Luebbe, Germany). Chl-a was determined using a fluorometer (Turner Designs, San Jose, CA, USA) after extraction in 90% acetone in the dark for 24h at 4°C. The multi-parameter water quality detector (YSI, Yellow Springs, OH, USA) was used to measure temperature and salinity in situ [5]. Based on the validated hydrodynamic model, the water quality model shows a good agreement between the measured and simulated results at various sampling locations (Figure 3). Relative error is used to quantify the differences between model and in situ measurements. The mean relative errors for NH_4-N, NO_3-N, PO_4-P, and Chl-a are 21%, 10%, 13% and 17%, respectively. The mean relative errors for temperature and salinity are 3.4% and 1.7%, respectively. Overall, the model performs well for the fate and transport of nutrients in Jinmeng Bay.

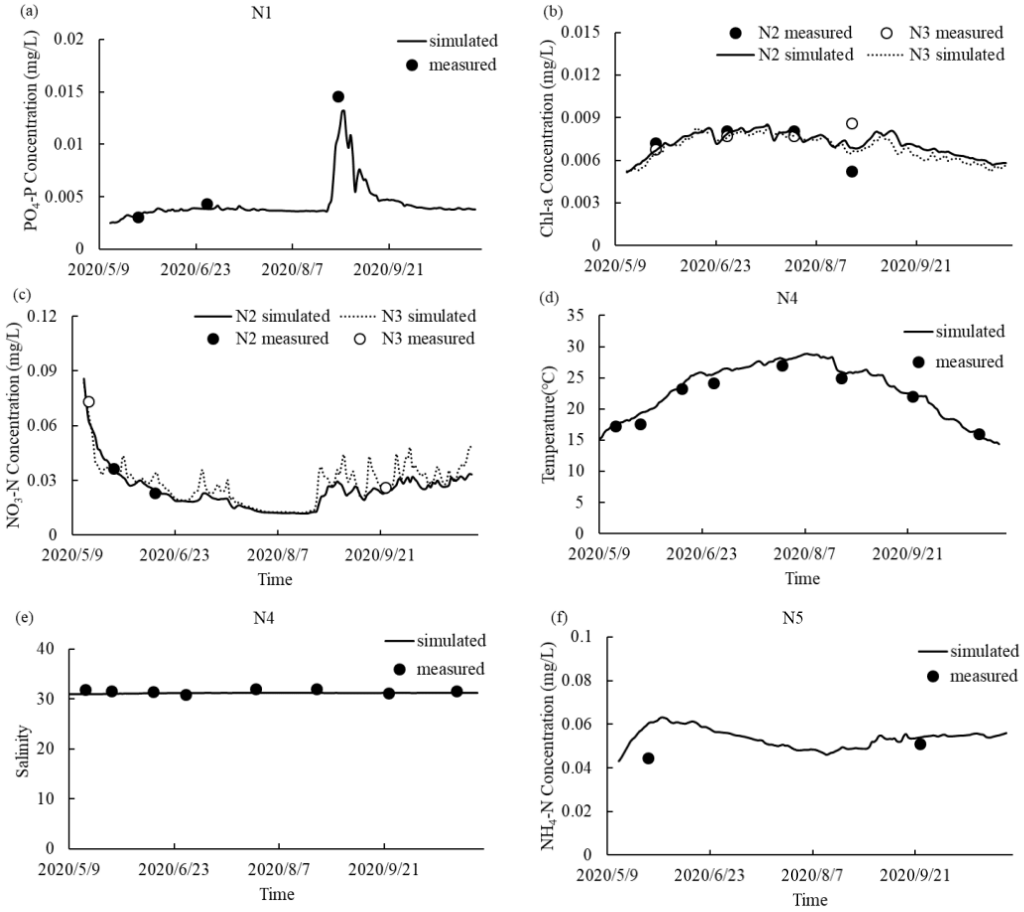

Figure 3. Measured and simulated (**a**) PO_4-P concentration, (**b**) Chl-a concentration, (**c**) NO_3-N concentration, (**d**) temperature (**e**) salinity, and (**f**) NH_4-N concentration in Jinmeng Bay.

3. Results

3.1. Spatiotemporal Distribution of Nutrients in Jinmeng Bay

In Jinmeng Bay and the adjacent area, the current flows southwest with a maximum velocity of 0.26 m/s during the flood tides, and northeast at about 0.23 m/s during the ebb tides. The artificial islands slow down the current speeds (below 0.06 m/s) in the nearshore areas. All nutrients vary spatially and temporally due to the differences in terrestrial inputs and hydrodynamic transport (Figure 4). The concentrations of NO_3-N, NH_4-N, and PO_4-P decrease gradually from the river estuary to the offshore region. The simulated results show that nutrient transport in Jinmeng Bay is driven by tides and currents to the northwest side of the islands during flood tides. While during ebb tides, nutrients are transported in a northeast direction and accumulate in the estuary. High nutrient levels in Jinmeng Bay are mainly attributed to the influx of pollutants from the Tanghe River instead of the Xinkaihe or Xinhe Rivers. Due to the influence of artificial islands, nutrients tend to accumulate in the coastal areas of Jinmeng Bay with weak hydrodynamics and slow water exchange. In addition to a sufficient nutrient supply, suitable water temperatures and salinities were also critical for the green algae blooms. The average water temperature and salinity of Jinmeng Bay was 23 °C and 31.3 in June 2020 (Figure 5).

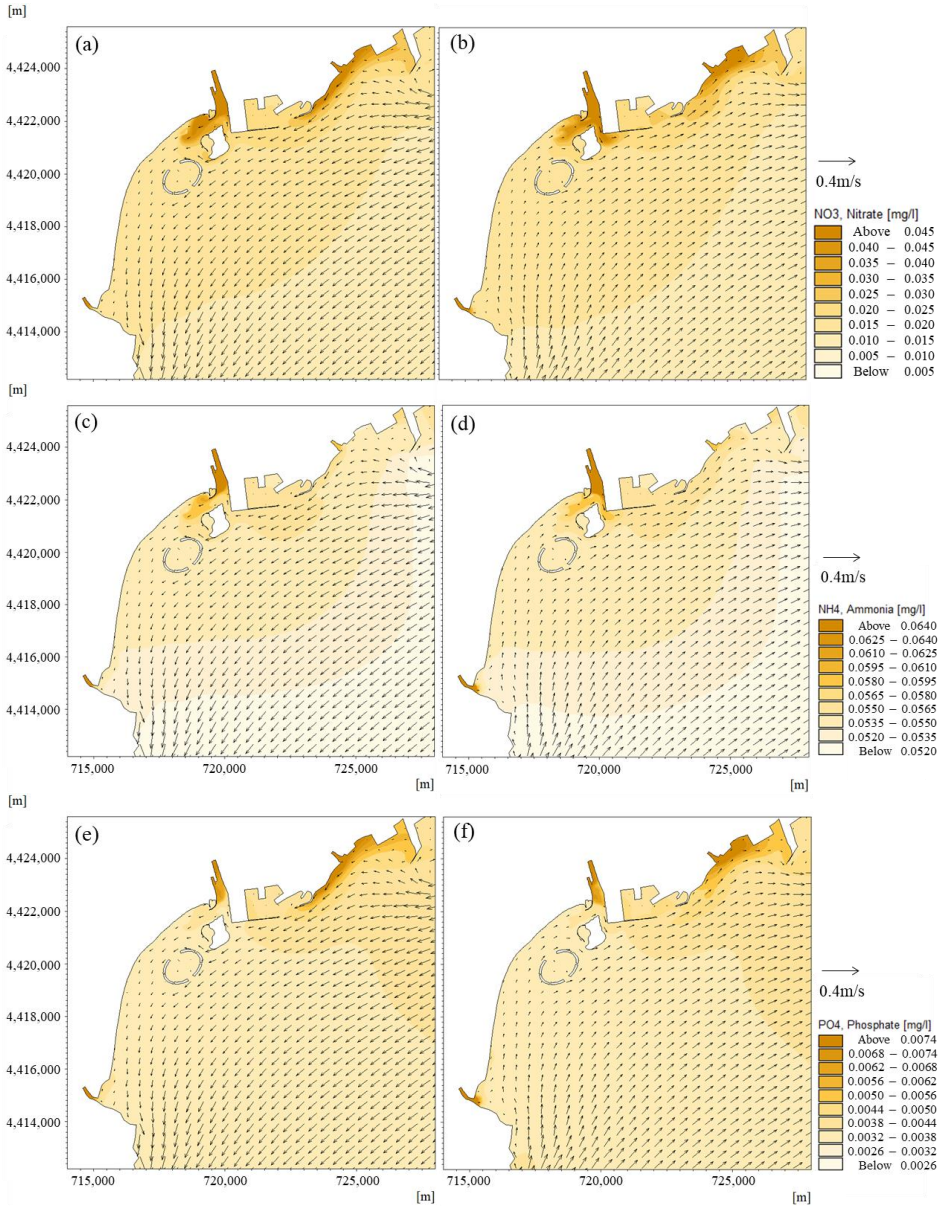

Figure 4. Modeled currents and distributions of NO_3-N (**a**,**b**), NH_4-N (**c**,**d**), and PO_4-P (**e**,**f**) at peak flood (**a**,**c**,**e**) and peak ebb (**b**,**d**,**f**).

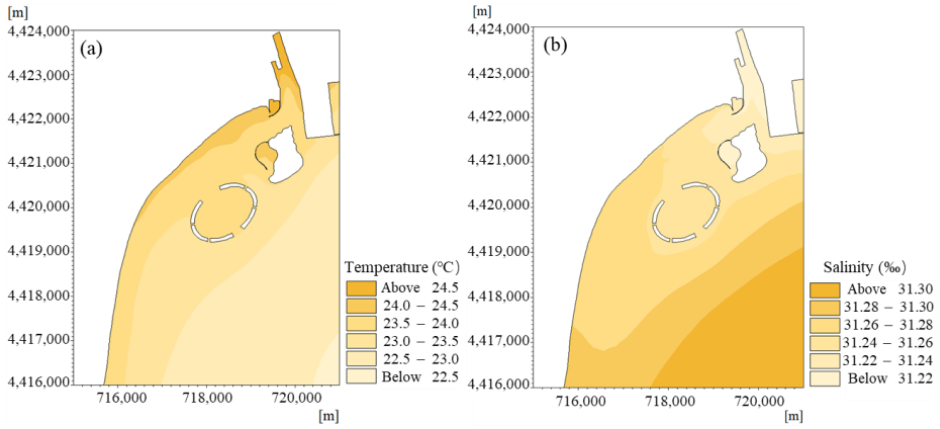

Figure 5. Simulated spatial distribution of (**a**) temperature and (**b**) salinity in June 2020.

The monthly averaged distribution of nutrients in June and July 2020 in Figure 6 indicates that NH_4-N and NO_3-N decreased by 15% and 11% in Jinmeng Bay from June to July 2020, which was related to the fluctuating decline of pollutant input from the Tanghe River (Figure 7). However, the temporal variation in PO_4-P concentration in July was similar to that in June. High PO_4-P is evident near the port jetty on the northeast side of Tanghe River due to the fact that the nutrient flux of PO_4-P from Xinkaihe River is about 3 orders of magnitude larger than that from Tanghe River. Figure 8 compared the spatiotemporal variations of NO_3-N on 10 September and 30 October, with the wind blowing north and southwest, respectively. A high NO_3-N zone extended from the Tanghe River estuary to Jinshanzui under a north wind, while the sea area around the artificial islands had high NO_3-N values under a southwest wind. Under different wind conditions, the distribution of nutrient concentrations changed greatly, indicating that wind fields directly affect the distributions of pollutants, which are subsequently analyzed in the discussion.

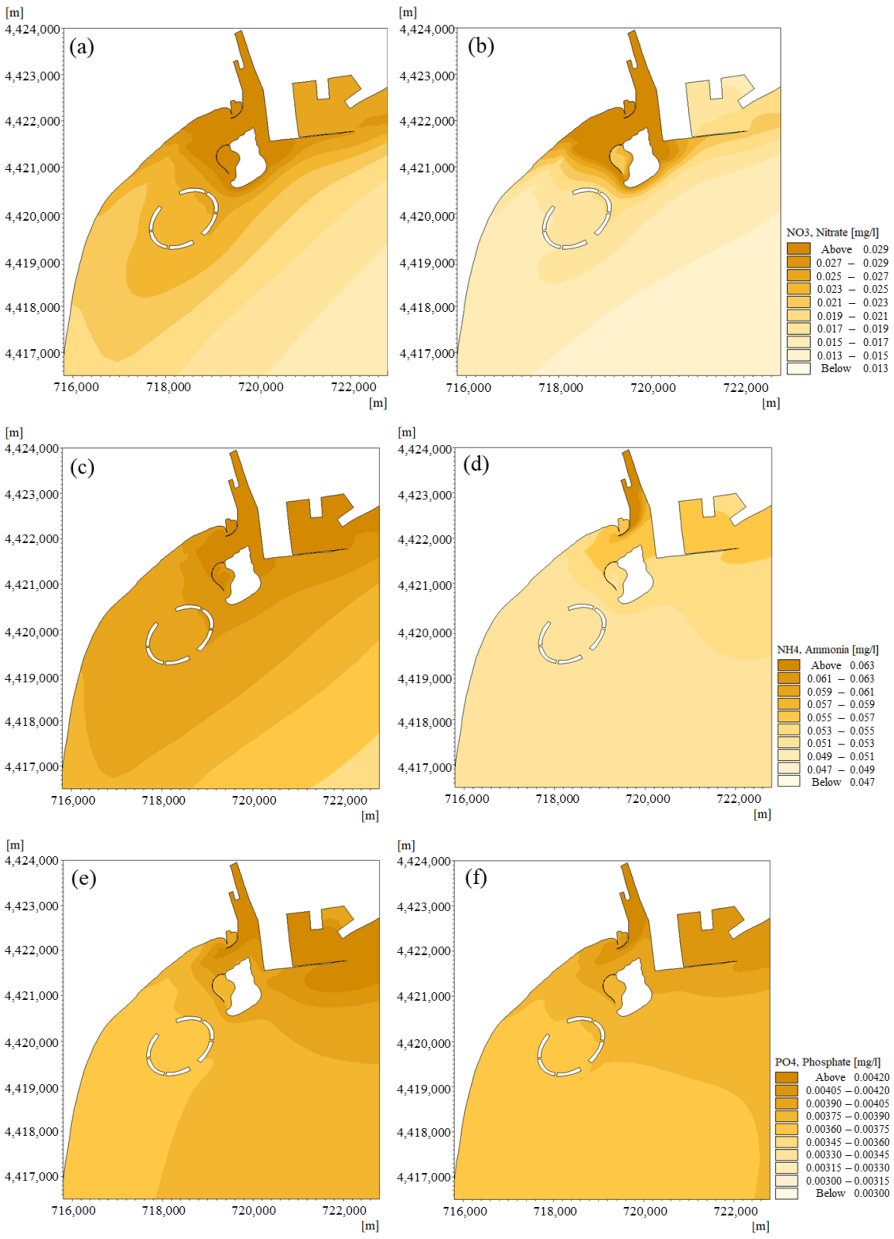

Figure 6. Modeled monthly averaged NO_3-N (**a**,**b**), NH_4-N (**c**,**d**), and PO_4-P (**e**,**f**) concentrations in June (**a**,**c**,**e**) and July (**b**,**d**,**f**) 2020 in Jinmeng Bay.

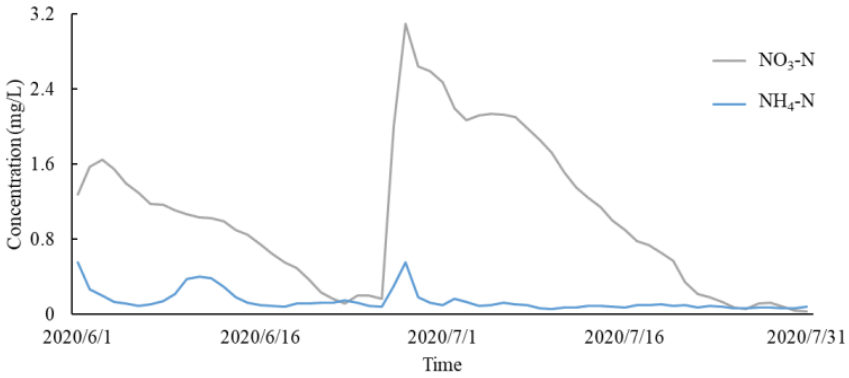

Figure 7. Variations in NO_3-N and NH_4-N concentrations in the Tanghe River in June and July 2020.

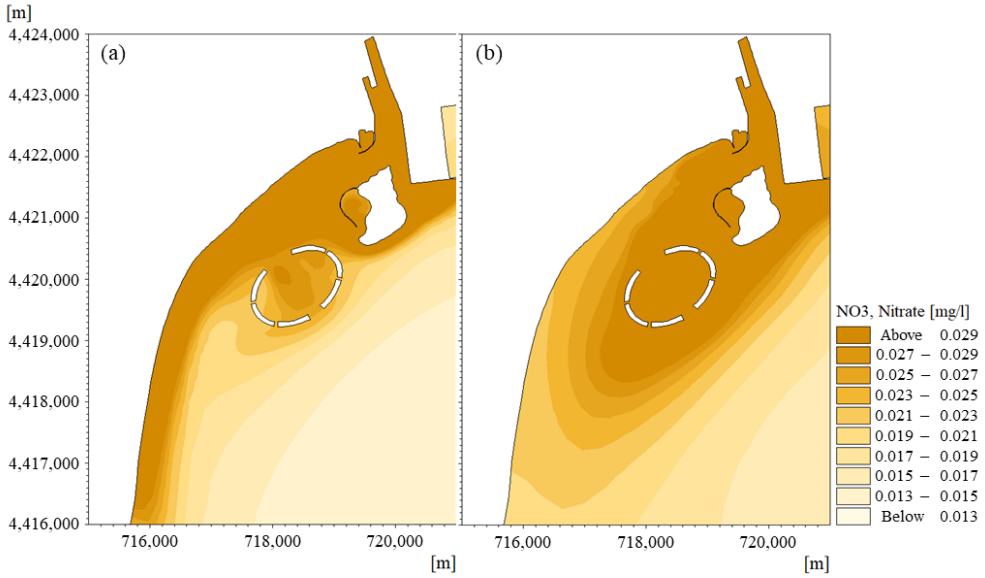

Figure 8. Modeled NO_3-N concentrations on (**a**) 10 September and (**b**) 30 October 2020, in Jinmeng Bay.

3.2. Spatiotemporal Distribution of Chlorophyll-a in Jinmeng Bay

Nutrients are essential for the growth and propagation of green algae [41–44]. Using a horizontal trawling sampling method modified from Wang et al. [45], field observations of floating macroalgae were conducted at the following three locations (Figure 1): M1 (39.901 N, 119.552 E), M2 (39.895 N, 119.543 E), and M3 (39.890 N, 119.536 E). In June, the average biomass of green-tide algae in the water of Jinmeng Bay was the highest, at 799.3 g/m^3, while in July it was only 151.5 g/m^3 [5], indicating that the biomass of floating macroalgae in Jinmeng Bay decreased significantly in July 2020 (Figure 9). Considering that Chl-a is a commonly used indicator for algal biomass [8], the spatiotemporal distribution of simulated Chl-a concentrations is shown in Figure 10 for the date of the field survey (Figure 9). The area where the simulated Chl-a concentration changes is the same as where the green-tide algae is distributed. The concentrations of Chl-a increase from early June to mid-June and then reach their maximum on June 29. However, Chl-a concentrations decrease sharply on July 18, especially in the coastal areas of Jinmeng Bay, and remain at a lower level until the end of July. On July 27, the Chl-a concentrations recover slightly in the inshore waters. In general, the overall model's results match not only the field observations with reference to the spatial distribution trends, but also those related to green tide dynamics changes in Jinmeng Bay. Field surveys can only present the biomass at the measurement point (limited by the number of sampling stations and sampling time), whereas numerical simulations can clearly show the spatio-temporal changes in Chl-a. For instance, the biomass of floating macroalgae on July 18 and July 19 is only 67.5 g/m^3 and

83.8 g/m^3, respectively, and the simulated Chl-a concentration also keeps decreasing from 0.0083 mg/L to 0.0070 mg/L in coastal shallow waters.

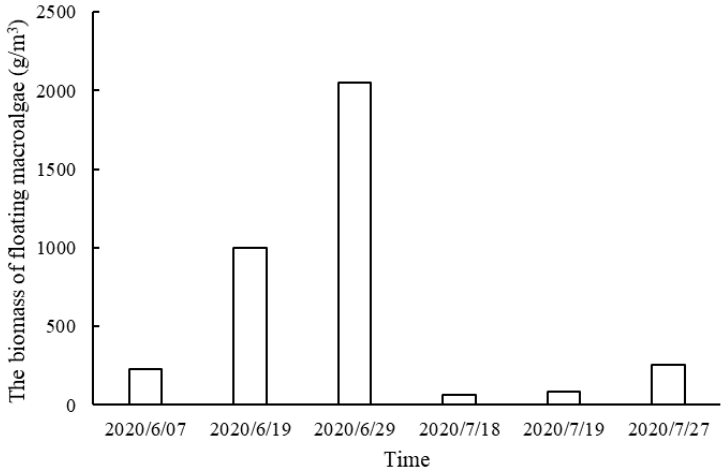

Figure 9. Biomass of green-tide algae in Jinmeng Bay in June and July 2020.

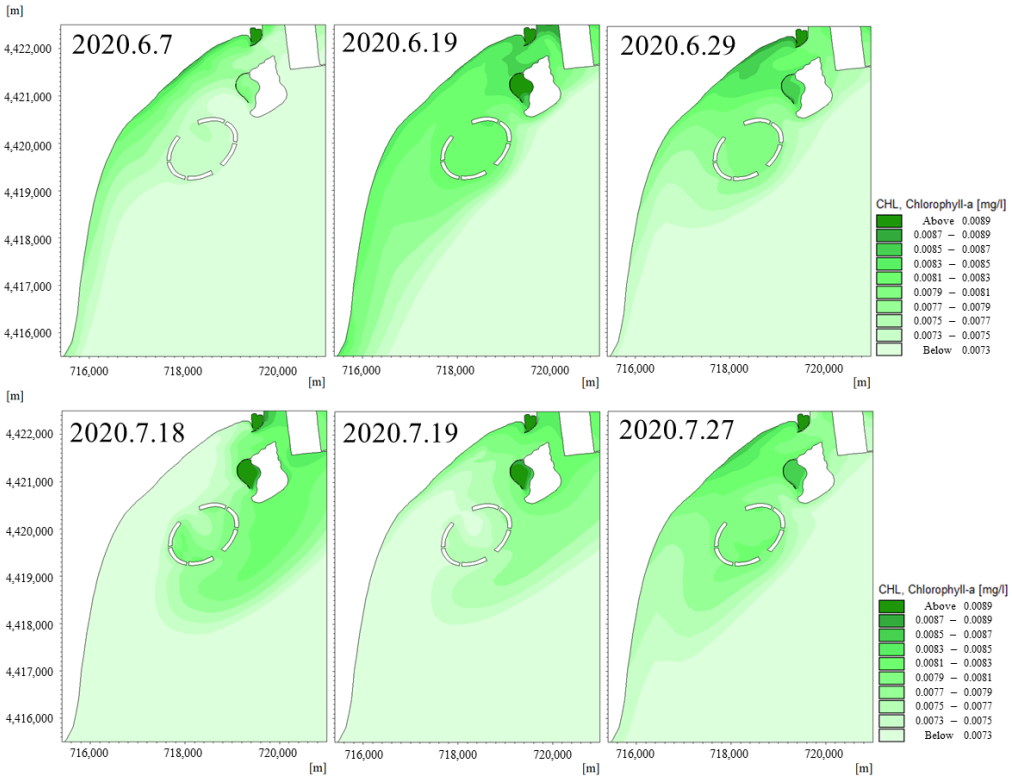

Figure 10. Daily averaged simulated Chl-a concentration in Jinmeng Bay in June and July 2020.

4. Discussion

In 2020, the green algae blooming scales shrank sharply compared to those in previous years, which may be attributed to several factors. Han et al. [5] found that the amount of micro-propagules and attached green algae decreased significantly in July 2020. Here, we mainly focus on the river input and wind forcing for the green tides in Jinmeng Bay.

4.1. Key Nutrient Inputs from Tanghe River

Numerous studies have shown that nutrients play a dominant role in Chl-a levels [16,46–48]. Nitrogen and phosphorus are of vital importance in affecting the growth of green algae [1,49]. To reveal the dynamic change in water quality, the mean annual concentrations of total nitrogen and total phosphorus in the Tanghe River from 2013 to 2020 are shown in Figure 11. Total phosphorus concentrations were relatively stable during 2013–2020 and fluctuated at around 0.1 mg/L, which could meet Class II or III of the Chinese Surface Water Quality Standard [50]. However, total nitrogen concentrations were always worse than Class V, peaking in 2016 with the maximum value of 5.34 mg/L. The high nutrient levels boost the blooms of green-tide algae in Jinmeng Bay. This suggests that the increased rate of total phosphorus input is much slower than that of total nitrogen, and the excessive total nitrogen input from the Tanghe River plays a major role in the eutrophic processes of Jinmeng Bay coastal waters. Due to effective governmental management of river pollution, the concentration of total nitrogen shows a sharp decrease in the Tanghe River in 2020.

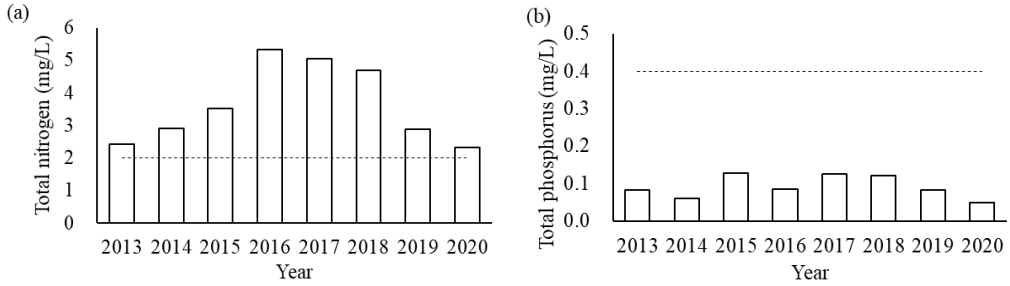

Figure 11. Annual variations in (**a**) total nitrogen and (**b**) total phosphorus concentrations from 2013 to 2020 in the Tanghe River. The black dashed line represents Class V of the Chinese Surface Water Quality Standard.

Han et al. [5] pointed out that the biomass of attached and floating macroalgae was significantly lower during the green tide bloom in 2020, especially in July, compared to those in the previous years. Figure 12a shows the comparison of the biomass of green-tide algae in July 2018 and 2020. Apparently, the interannual differences in the biomass of green tides may be related to variations in nutrients. As shown in Figure 12b–d, fluxes in NH_4-N and PO_4-P decreased by 71% and 69% from July 2018 to 0.381 t and 0.035 t in 2020. The fluxes of NO3-N were 6.40 t in July 2018 and 4.59 t in July 2020. These data indicate that the fluxes of all nutrients decreased significantly from July 2018 to July 2020. Moreover, a large amount of NO_3-N, a dominant component of dissolved inorganic nitrogen in the Tanghe River (Figure 12), provides a sufficient nutritional environment for macroalgae blooms to occur. This conclusion is supported by the study of Han et al. [5]. Figure 13 shows the variations in the nutrient concentration and river discharge of the Tanghe River. There were little changes in the river discharge between 2018 and 2020. However, the nutrient concentration was higher during July 2018, indicating that nutrient loading from the Tanghe River was most likely affected by anthropogenic input. At the same time, compared to June 2020, lower nutrient concentrations in Jinmeng Bay due to reduced loads from the Tanghe River contributed to a reduction in the Chl-a concentration in July (Figures 6 and 10). Generally, a lower nutrient supply may limit algae growth which, in turn, reduces Chl-a. The overall decreasing pattern of Chl-a in Jinmeng Bay in 2020 is mainly attributed to a substantial reduction in the nutrient loads of the Tanghe River.

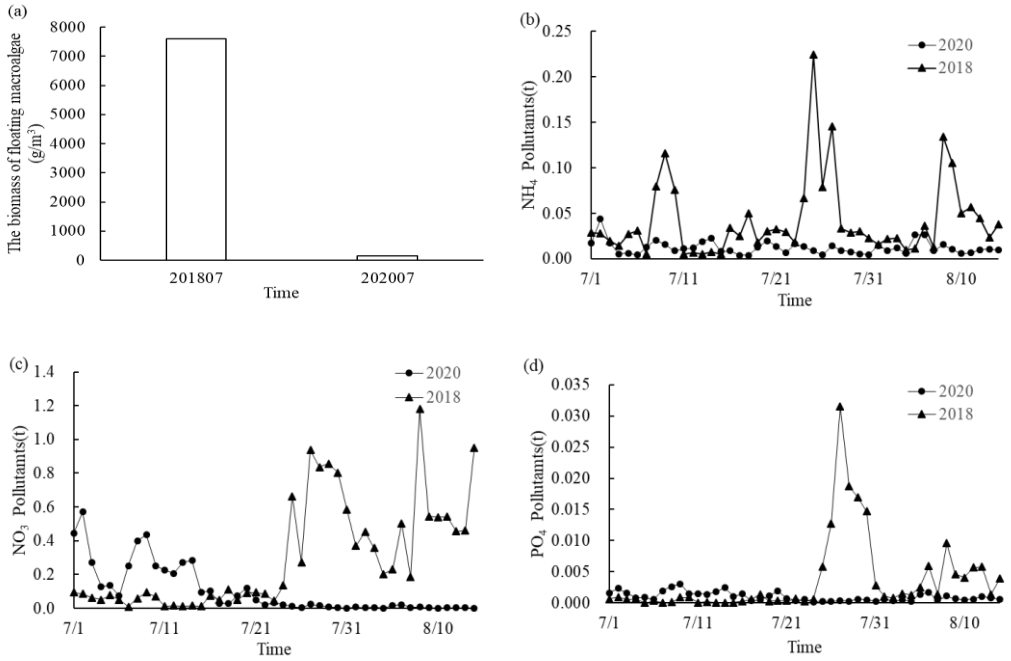

Figure 12. Comparison of (**a**) the biomass of floating macroalgae, (**b**) NH_4-N flux, (**c**) NO_3-N flux, and (**d**) PO_4-P flux in July 2018 and 2020.

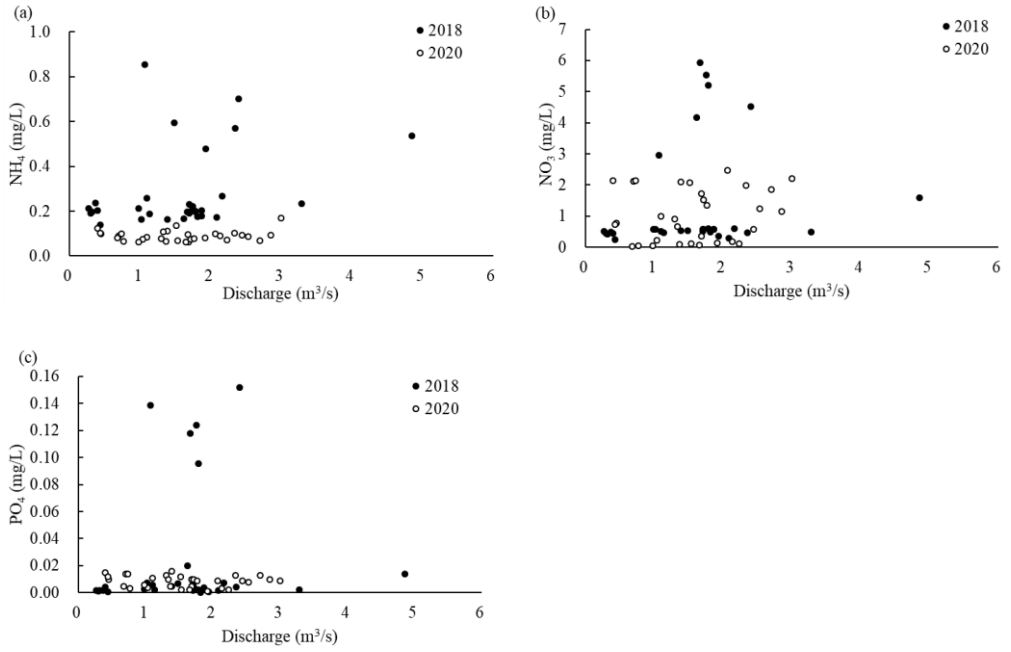

Figure 13. Variations in (**a**) NH_4-N concentration and river discharge, (**b**) NO_3-N concentration and river discharge, and (**c**) PO_4-P concentration and river discharge in July 2018 and 2020.

4.2. Effect of Wind on Chlorophyll-a Variability in Jinmeng Bay

Besides eutrophication, wind is another important contributing factor for the distribution and variability of Chl-a [42,51–53]. Figure 14a,b compares the monthly average wind field in July 2018 and 2020. In July 2018, the wind in Jinmeng Bay blew from the southeast, while in 2020, the wind kept blowing from the west, and there was little change in wind speed between the two years (with an average wind speed of 2.0 m/s and 2.3 m/s in July 2018 and 2020, respectively). As shown in Figure 14c, the prevailing wind directions are from WSW to ESE, which accounted for 66% of the data during 2018–2022. Hence, we

use southeasterly, southerly, and southwesterly wind as the representative wind in the following analysis to investigate the effect of wind direction on Chl-a variability in Jinmeng Bay. The simulation was carried out with a constant wind speed of 5.5 m/s since about 57% wind speeds are between 3.4 and 5.5 m/s and 5.5 and 8 m/s (Figure 14c). The field observations in 2020 were adapted to the river input. The model's results revealed that Chl-a displayed significant spatial variation under different wind directions (Figure 15). When southeasterly winds prevail, there are higher Chl-a concentrations in Jinmeng Bay (Figure 15c). In contrast, southwesterly winds are more likely to suppress the supply of nutrition from the Tanghe River to the coastal areas, thereby reducing Chl-a concentrations in Jinmeng Bay (Figure 15a). Under southerly winds, Chl-a levels are in between the above two scenarios (Figure 15b). The average concentrations of Chl-a in the seaweed beds under southwesterly, southerly, and southeasterly wind are 0.0050 mg/L, 0.0053 mg/L and 0.0076 mg/L, respectively.

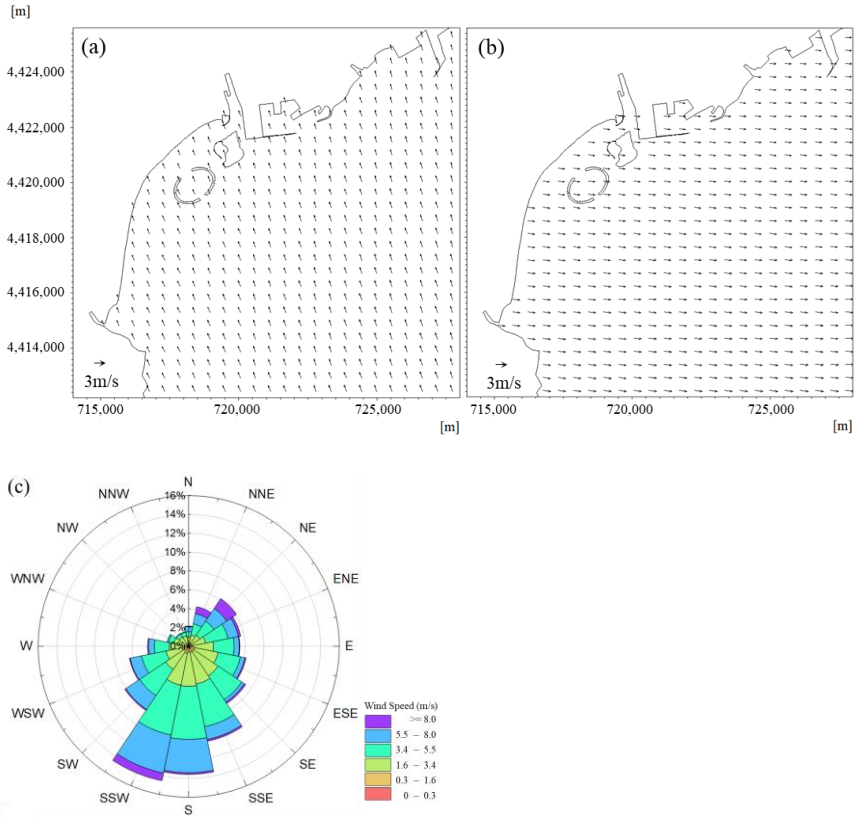

Figure 14. Monthly averaged wind in July (**a**) 2018, (**b**) 2020, and (**c**) the wind rose during 2018–2022.

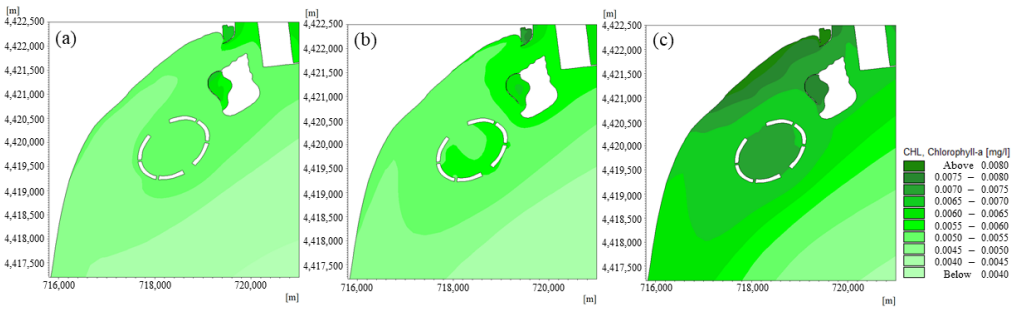

Figure 15. Spatial distribution of simulated Chl-a concentrations under (**a**) southwesterly, (**b**) southerly, and (**c**) southeasterly wind.

Residual current is especially critical for sediment transport and pollutant dispersion [54–57]. In order to further understand the effects of wind on the distribution of pollutants in a semi-enclosed domain with multiple artificial structures, the wind-induced residual current was calculated under different wind directions (Figure 16). The model's conditions are consistent with those in previous simulations (Figure 15). The model's results revealed that the variations in wind direction alter both the speed and direction of the residual current. As shown in Figure 16a,b, under winds predominantly from the south and southwest, residual currents flow in a predominantly northeastward direction along the coast, which hinders the influx of nutrients from Tanghe River and therefore lowers the Chl-a levels. Under southeasterly winds, a small residual current (0.02 m/s) occurs near the seaweed beds due to flow attenuation by the canopy of the vegetation and artificial islands and reefs [58–61], resulting in a long residence time and relatively weak seawater exchange capacity in this area compared to other areas in Jinmeng Bay. Thus, the southeasterly winds led to increased Chl-a concentrations near the seaweed beds. Similarly, substantial macroalgal piled up on the beaches under prevailing southeasterly winds during the field observations. In summary, the pollutant is more likely to accumulate in the coastal areas under southeast winds and migrate to offshore waters under southwest winds. This finding provides references for the pre-warning of green algae blooms in Jinmeng Bay.

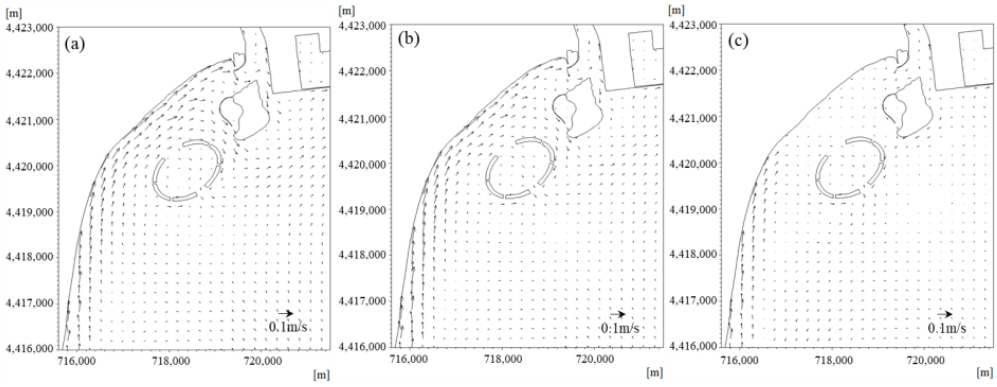

Figure 16. Modeled wind-induced residual current field in Jinmeng Bay under (**a**) southwesterly, (**b**) southerly, and (**c**) southeasterly wind.

5. Conclusions

The annual outbreaks of green tides in JMB since 2015 have affected local tourism and the coastal ecological environment. In this study, the driving impact of environmental factors on the distribution of Chl-a was investigated using field observations and numerical simulations. A hydrodynamic model together with a water quality model were established based on MIKE 21. Dramatically improved water quality and unique wind patterns are two main contributing factors for the change in Chl-a in 2020. The major conclusions are as follows:

(a) The model can reproduce the spatial and temporal distribution of nutrients and Chl-a in Jinmeng Bay well. A high Chl-a concentration along the coast in Jinmeng Bay indicates that the Tanghe River is the primary source of nutrients for Chl-a growth. The nutrients are more likely to accumulate in Jinmeng Bay mainly because the advection and diffusion of the pollutants are weakened by the presence of marine structures and seaweed beds.

(b) Abundant total nitrogen inputs provide a sufficient nutritious environment for macroalgae blooms. The total nitrogen concentration decreased continuously from 2016 to 2020. A reduction in riverine nutrient loads, especially NO_3-N, plays a dominant role in alleviating green tides. The declined nutrient inflow in Jinmeng Bay is the main driver of the Chl-a change in July 2020.

(c) Wind forcing is the controlling factor for the spatial distribution of Chl-a in Jinmeng Bay. Southwesterly winds suppress the inflow of nutrition from the Tanghe River to the coastal areas, and therefore lower the Chl-a levels. The opposite is true for southeasterly winds. This finding provides useful information for the mitigation of green tides in Jinmeng Bay and other similar regions.

Author Contributions: Conceptualization, C.K. and D.W.; methodology, C.K., D.W. and W.S.; software, D.W.; investigation, G.W., J.L. and R.X.; writing—original draft preparation, D.W.; writing—review and editing, C.K. and Q.Z.; supervision, C.K.; funding acquisition, C.K. All authors have read and agreed to the published version of the manuscript.

Funding: This research was funded by the National Key Research and Development Program of China, under contract no. 2022YFC3106205, and the National Key Research and Development Program of China, under contract no. 2019YFC1407902.

Institutional Review Board Statement: Not applicable.

Informed Consent Statement: Not applicable.

Data Availability Statement: Data are contained within the article.

Acknowledgments: We are sincerely grateful to the Key Laboratory of Marine Eco-Environmental Science and Technology, First Institute of Oceanography, Ministry of Natural Resources of People's Republic of China for supporting the fieldwork and measured data for the model validation.

Conflicts of Interest: The authors declare no conflicts of interest.

References

1. Zhang, Y.; He, P.; Li, H.; Li, G.; Liu, J.; Jiao, F.; Zhang, J.; Huo, Y.; Shi, X.; Su, R.; et al. *Ulva Prolifera* Green-Tide Outbreaks and Their Environmental Impact in the Yellow Sea, China. *Natl. Sci. Rev.* **2019**, *6*, 825–838. [CrossRef]
2. Shi, X.; Qi, M.; Tang, H.; Han, X. Spatial and Temporal Nutrient Variations in the Yellow Sea and Their Effects on Ulva Prolifera Blooms. *Estuar. Coast. Shelf Sci.* **2015**, *163*, 36–43. [CrossRef]
3. Wang, S.; Zhao, L.; Wang, Y.; Zhang, H.; Li, F.; Zhang, Y. Distribution Characteristics of Green Tides and Its Impact on Environment in the Yellow Sea. *Mar. Environ. Res.* **2022**, *181*, 105756. [CrossRef]
4. Song, W.; Wang, Z.; Li, Y.; Han, H.; Zhang, X. Tracking the Original Source of the Green Tides in the Bohai Sea, China. *Estuar. Coast. Shelf Sci.* **2019**, *219*, 354–362. [CrossRef]
5. Han, H.; Li, Y.; Ma, X.; Song, W.; Wang, Z.; Zhang, X. Factors Influencing the Spatial and Temporal Distributions of Green Algae Micro-Propagules in the Coastal Waters of Jinmenghaiwan, Qinhuangdao, China. *Mar. Pollut. Bull.* **2022**, *175*, 113328. [CrossRef]
6. Liu, Y.; Tang, D.; Tang, S.; Morozov, E.; Liang, W.; Sui, Y. A Case Study of Chlorophyll a Response to Tropical Cyclone Wind Pump Considering Kuroshio Invasion and Air-Sea Heat Exchange. *Sci. Total Environ.* **2020**, *741*, 140290. [CrossRef] [PubMed]
7. Li, D.; Gao, Z.; Wang, Y. Research on the Long-Term Relationship between Green Tide and Chlorophyll-a Concentration in the Yellow Sea Based on Google Earth Engine. *Mar. Pollut. Bull.* **2022**, *177*, 113574. [CrossRef]
8. Royer, T.V.; David, M.B.; Gentry, L.E.; Mitchell, C.A.; Starks, K.M.; Heatherly, T.; Whiles, M.R. Assessment of Chlorophyll-*a* as a Criterion for Establishing Nutrient Standards in the Streams and Rivers of Illinois. *J. Environ. Qual.* **2008**, *37*, 437–447. [CrossRef] [PubMed]
9. Harvey, E.T.; Kratzer, S.; Philipson, P. Satellite-Based Water Quality Monitoring for Improved Spatial and Temporal Retrieval of Chlorophyll-a in Coastal Waters. *Remote Sens. Environ.* **2015**, *158*, 417–430. [CrossRef]
10. Liu, K.-K.; Chao, S.-Y.; Shaw, P.-T.; Gong, G.-C.; Chen, C.-C.; Tang, T.Y. Monsoon-Forced Chlorophyll Distribution and Primary Production in the South China Sea: Observations and a Numerical Study. *Deep Sea Res. Part I Oceanogr. Res. Pap.* **2002**, *49*, 1387–1412. [CrossRef]
11. Zhang, W.; Wang, H.; Chai, F.; Qiu, G. Physical Drivers of Chlorophyll Variability in the Open South China Sea. *JGR Ocean.* **2016**, *121*, 7123–7140. [CrossRef]
12. Signorini, S.R.; Franz, B.A.; McClain, C.R. Chlorophyll Variability in the Oligotrophic Gyres: Mechanisms, Seasonality and Trends. *Front. Mar. Sci.* **2015**, *2*, 1. [CrossRef]
13. Liang, W.; Tang, D.; Luo, X. Phytoplankton Size Structure in the Western South China Sea under the Influence of a 'Jet-Eddy System'. *J. Mar. Syst.* **2018**, *187*, 82–95. [CrossRef]
14. Tang, D.; Kawamura, H.; Lee, M.-A.; Van Dien, T. Seasonal and Spatial Distribution of Chlorophyll-a Concentrations and Water Conditions in the Gulf of Tonkin, South China Sea. *Remote Sens. Environ.* **2003**, *85*, 475–483. [CrossRef]
15. Hong, L.; Wang, C.; Zhou, Y.; Chen, M.; Liu, H.; Lin, Z.; Song, X. The Distribution of Chlorophyll a in the Tropical Eastern Indian Ocean in Austral Summer. *Acta Oceanol. Sin.* **2012**, *31*, 146–159. [CrossRef]

16. Wang, Y.; Tian, X.; Gao, Z. Evolution of Satellite Derived Chlorophyll-a Trends in the Bohai and Yellow Seas during 2002–2018: Comparison between Linear and Nonlinear Trends. *Estuar. Coast. Shelf Sci.* **2021**, *259*, 107449. [CrossRef]
17. Kahru, M.; Gille, S.T.; Murtugudde, R.; Strutton, P.G.; Manzano-Sarabia, M.; Wang, H.; Mitchell, B.G. Global Correlations between Winds and Ocean Chlorophyll. *J. Geophys. Res.* **2010**, *115*, 2010JC006500. [CrossRef]
18. Nababan, B.; Muller-Karger, F.E.; Hu, C.; Biggs, D.C. Chlorophyll Variability in the Northeastern Gulf of Mexico. *Int. J. Remote Sens.* **2011**, *32*, 8373–8391. [CrossRef]
19. Chen, G.; Xiu, P.; Chai, F. Physical and Biological Controls on the Summer Chlorophyll Bloom to the East of Vietnam. *J. Ocean.* **2014**, *70*, 323–328. [CrossRef]
20. Martins, I.; Marques, J.C. A Model for the Growth of Opportunistic Macroalgae (*Enteromorpha* sp.) in Tidal Estuaries. *Estuar. Coast. Shelf Sci.* **2002**, *55*, 247–257. [CrossRef]
21. Sun, K.; Ren, J.S.; Bai, T.; Zhang, J.; Liu, Q.; Wu, W.; Zhao, Y.; Liu, Y. A Dynamic Growth Model of Ulva Prolifera: Application in Quantifying the Biomass of Green Tides in the Yellow Sea, China. *Ecol. Model.* **2020**, *428*, 109072. [CrossRef]
22. Long, T.; Wu, L.; Meng, G.; Guo, W. Numerical Simulation for Impacts of Hydrodynamic Conditions on Algae Growth in Chongqing Section of Jialing River, China. *Ecol. Model.* **2011**, *222*, 112–119. [CrossRef]
23. Li, K.; Zhang, L.; Li, Y.; Zhang, L.; Wang, X. A Three-Dimensional Water Quality Model to Evaluate the Environmental Capacity of Nitrogen and Phosphorus in Jiaozhou Bay, China. *Mar. Pollut. Bull.* **2015**, *91*, 306–316. [CrossRef] [PubMed]
24. Chen, Y.; Song, D.; Li, K.; Gu, L.; Wei, A.; Wang, X. Hydro-Biogeochemical Modeling of the Early-Stage Outbreak of Green Tide (*Ulva prolifera*) Driven by Land-Based Nutrient Loads in the Jiangsu Coast. *Mar. Pollut. Bull.* **2020**, *153*, 111028. [CrossRef] [PubMed]
25. Mendes, J.; Ruela, R.; Picado, A.; Pinheiro, J.P.; Ribeiro, A.S.; Pereira, H.; Dias, J.M. Modeling Dynamic Processes of Mondego Estuary and Óbidos Lagoon Using Delft3D. *JMSE* **2021**, *9*, 91. [CrossRef]
26. Gao, Q.; He, G.; Fang, H.; Bai, S.; Huang, L. Numerical Simulation of Water Age and Its Potential Effects on the Water Quality in Xiangxi Bay of Three Gorges Reservoir. *J. Hydrol.* **2018**, *566*, 484–499. [CrossRef]
27. Cruz-Rico, J.; Rivas, D. Physical and Biogeochemical Variability in Todos Santos Bay, Northwestern Baja California, Derived from a Numerical NPZD Model. *J. Mar. Syst.* **2018**, *183*, 63–75. [CrossRef]
28. Yu, L.; Yang, B.; Jiang, W.; Li, K. A Model Study on Dynamical Processes of Phytoplankton in Laizhou Bay. *J. Ocean Univ. China* **2014**, *13*, 23–31. [CrossRef]
29. Feng, L.; Chen, B.; Hayat, T.; Alsaedi, A.; Ahmad, B. Modelling the Influence of Thermal Discharge under Wind on Algae. *Phys. Chem. Earth Parts A/B/C* **2015**, *79–82*, 108–114. [CrossRef]
30. Lopes, J.F.; Silva, C. Temporal and Spatial Distribution of Dissolved Oxygen in the Ria de Aveiro Lagoon. *Ecol. Model.* **2006**, *197*, 67–88. [CrossRef]
31. MIKE 21. *Hydrodynamic and Transport Module Scientific Documentation*; MIKE 21 Flow Model FM; MIKE by DHI: Copenhagen, Denmark, 2014.
32. Ranjbar, M.H.; Etemad-Shahidi, A.; Kamranzad, B. Modeling the Combined Impact of Climate Change and Sea-Level Rise on General Circulation and Residence Time in a Semi-Enclosed Sea. *Sci. Total Environ.* **2020**, *740*, 140073. [CrossRef]
33. Kuang, C.; Chen, J.; Wang, J.; Qin, R.; Fan, J.; Zou, Q. Effect of Wind-Wave-Current Interaction on Oil Spill in the Yangtze River Estuary. *J. Mar. Sci. Eng.* **2023**, *11*, 494. [CrossRef]
34. Jakacki, J.; Przyborska, A.; Kosecki, S.; Sundfjord, A.; Albretsen, J. Modelling of the Svalbard Fjord Hornsund. *Oceanologia* **2017**, *59*, 473–495. [CrossRef]
35. Doan, Q.T.; Nguyen, T.M.L.; Quach, T.T.T.; Tran, A.P.; Nguyen, C.D. Assessment of Water Quality in Coastal Estuaries under the Impact of an Industrial Zone in Hai Phong, Vietnam. *Phys. Chem. Earth Parts A/B/C* **2019**, *113*, 100–114. [CrossRef]
36. Jia, H.; Shen, Y.; Su, M.; Yu, C. Numerical Simulation of Hydrodynamic and Water Quality Effects of Shoreline Changes in Bohai Bay. *Front. Earth Sci.* **2018**, *12*, 625–639. [CrossRef]
37. Han, X.; Kuang, C.; Li, Y.; Song, W.; Qin, R.; Wang, D. Numerical Modeling of a Green Tide Migration Process with Multiple Artificial Structures in the Western Bohai Sea, China. *Appl. Sci.* **2022**, *12*, 3017. [CrossRef]
38. Shalby, A.; Elshemy, M.; Zeidan, B.A. Assessment of Climate Change Impacts on Water Quality Parameters of Lake Burullus, Egypt. *Environ. Sci. Pollut. Res.* **2020**, *27*, 32157–32178. [CrossRef] [PubMed]
39. Islam, M.M.M.; Iqbal, M.S.; Leemans, R.; Hofstra, N. Modelling the Impact of Future Socio-Economic and Climate Change Scenarios on River Microbial Water Quality. *Int. J. Hyg. Environ. Health* **2018**, *221*, 283–292. [CrossRef]
40. Zhu, Y.P.; Zhang, H.P.; Chen, L.; Zhao, J.F. Influence of the South–North Water Diversion Project and the Mitigation Projects on the Water Quality of Han River. *Sci. Total Environ.* **2008**, *406*, 57–68. [CrossRef]
41. Yadav, A.; Pandey, J. The Pattern of N/P/Si Stoichiometry and Ecological Nutrient Limitation in Ganga River: Up- and Downstream Urban Influences. *Appl. Water Sci.* **2018**, *8*, 94. [CrossRef]
42. Yu, Y.; Xing, X.; Liu, H.; Yuan, Y.; Wang, Y.; Chai, F. The Variability of Chlorophyll-a and Its Relationship with Dynamic Factors in the Basin of the South China Sea. *J. Mar. Syst.* **2019**, *200*, 103230. [CrossRef]
43. Liu, X.; Wang, Z.; Zhang, X. A Review of the Green Tides in the Yellow Sea, China. *Mar. Environ. Res.* **2016**, *119*, 189–196. [CrossRef]
44. Liu, D.; Keesing, J.K.; He, P.; Wang, Z.; Shi, Y.; Wang, Y. The World's Largest Macroalgal Bloom in the Yellow Sea, China: Formation and Implications. *Estuar. Coast. Shelf Sci.* **2013**, *129*, 2–10. [CrossRef]

45. Wang, Z.; Xiao, J.; Fan, S.; Li, Y.; Liu, X.; Liu, D. Who Made the World's Largest Green Tide in China? An Integrated Study on the Initiation and Early Development of the Green Tide in Y Ellow S Ea. *Limnol. Oceanogr.* **2015**, *60*, 1105–1117. [CrossRef]
46. Zhao, L.; Zhu, R.; Zhou, Q.; Jeppesen, E.; Yang, K. Trophic Status and Lake Depth Play Important Roles in Determining the Nutrient-Chlorophyll a Relationship: Evidence from Thousands of Lakes Globally. *Water Res.* **2023**, *242*, 120182. [CrossRef]
47. Corredor-Acosta, A.; Cortés-Chong, N.; Acosta, A.; Pizarro-Koch, M.; Vargas, A.; Medellín-Mora, J.; Saldías, G.S.; Echeverry-Guerra, V.; Gutiérrez-Fuentes, J.; Betancur-Turizo, S. Spatio-Temporal Variability of Chlorophyll-A and Environmental Variables in the Panama Bight. *Remote Sens.* **2020**, *12*, 2150. [CrossRef]
48. Wang, Y.; Gao, Z. Contrasting Chlorophyll-a Seasonal Patterns between Nearshore and Offshore Waters in the Bohai and Yellow Seas, China: A New Analysis Using Improved Satellite Data. *Cont. Shelf Res.* **2020**, *203*, 104173. [CrossRef]
49. Li, H.; Zhang, Y.; Han, X.; Shi, X.; Rivkin, R.B.; Legendre, L. Growth Responses of Ulva Prolifera to Inorganic and Organic Nutrients: Implications for Macroalgal Blooms in the Southern Yellow Sea, China. *Sci. Rep.* **2016**, *6*, 26498. [CrossRef] [PubMed]
50. *GB3838-2002*; Chinese Environmental Water Quality Standards for Surface Water. Environmental Protection Agency of China: Beijing, China, 2002.
51. Setiawan, R.Y.; Habibi, A. Satellite Detection of Summer Chlorophyll-a Bloom in the Gulf of Tomini. *IEEE J. Sel. Top. Appl. Earth Obs. Remote Sens.* **2011**, *4*, 944–948. [CrossRef]
52. Muskananfola, M.R.; Jumsar; Wirasatriya, A. Spatio-Temporal Distribution of Chlorophyll-a Concentration, Sea Surface Temperature and Wind Speed Using Aqua-Modis Satellite Imagery over the Savu Sea, Indonesia. *Remote Sens. Appl. Soc. Environ.* **2021**, *22*, 100483. [CrossRef]
53. Shen, C.; Yan, Y.; Zhao, H.; Pan, J.; Devlin, A.T. Influence of Monsoonal Winds on Chlorophyll-α Distribution in the Beibu Gulf. *PLoS ONE* **2018**, *13*, e0191051. [CrossRef] [PubMed]
54. Gong, W.; Shen, J.; Jia, J. The Impact of Human Activities on the Flushing Properties of a Semi-Enclosed Lagoon: Xiaohai, Hainan, China. *Mar. Environ. Res.* **2008**, *65*, 62–76. [CrossRef] [PubMed]
55. Li, C.; O'Donnell, J. Tidally Driven Residual Circulation in Shallow Estuaries with Lateral Depth Variation. *J. Geophys. Res.* **1997**, *102*, 27915–27929. [CrossRef]
56. Xu, P.; Mao, X.; Jiang, W. Mapping Tidal Residual Circulations in the Outer Xiangshan Bay Using a Numerical Model. *J. Mar. Syst.* **2016**, *154*, 181–191. [CrossRef]
57. Liu, Z.; Wei, H.; Liu, G.; Zhang, J. Simulation of Water Exchange in Jiaozhou Bay by Average Residence Time Approach. *Estuar. Coast. Shelf Sci.* **2004**, *61*, 25–35. [CrossRef]
58. Chen, H.; Zou, Q.-P. Eulerian–Lagrangian Flow-Vegetation Interaction Model Using Immersed Boundary Method and OpenFOAM. *Adv. Water Resour.* **2019**, *126*, 176–192. [CrossRef]
59. Chen, H.; Liu, X.; Zou, Q.-P. Wave-Driven Flow Induced by Suspended and Submerged Canopies. *Adv. Water Resour.* **2019**, *123*, 160–172. [CrossRef]
60. Zhu, L.; Zou, Q.; Huguenard, K.; Fredriksson, D.W. Mechanisms for the Asymmetric Motion of Submerged Aquatic Vegetation in Waves: A Consistent-Mass Cable Model. *JGR Oceans* **2020**, *125*, e2019JC015517. [CrossRef]
61. Peng, Z.; Zou, Q.-P.; Lin, P. A Partial Cell Technique for Modeling the Morphological Change and Scour. *Coast. Eng.* **2018**, *131*, 88–105. [CrossRef]

Disclaimer/Publisher's Note: The statements, opinions and data contained in all publications are solely those of the individual author(s) and contributor(s) and not of MDPI and/or the editor(s). MDPI and/or the editor(s) disclaim responsibility for any injury to people or property resulting from any ideas, methods, instructions or products referred to in the content.